IEEE Access
Multidisciplinary ⋮ Rapid Review ⋮ Open Access Journal

Received 3 March 2024, accepted 13 March 2024, date of publication 1 April 2024, date of current version 29 April 2024.

Digital Object Identifier 10.1109/ACCESS.2024.3383788

TOPICAL REVIEW

Varactor-Based Continuously Tunable Microstrip Bandpass Filters: A Review, Issues and Future Trends

MENGJIE QIN[1,2,3], ZHONGMAO LI[1,2,3], (Member, IEEE), ZHIPENG REN[1,2], PENGZHAN LIU[1,2], (Student Member, IEEE), LANLAN LIAO[1,4], XIN QIU[1,2], AND ZHIQIANG LI[1,2,3], (Member, IEEE)

[1]Institute of Microelectronics, Chinese Academy of Sciences, Beijing 100029, China
[2]University of Chinese Academy of Sciences, Beijing 101408, China
[3]State Key Laboratory of Fabrication Technologies for Integrated Circuits, Beijing 100029, China
[4]Henan Institute of Advanced Technology, Zhengzhou University, Zhengzhou 450052, China

Corresponding authors: Zhongmao Li (lizhongmao@ime.ac.cn) and Zhiqiang Li (lizhiqiang@ime.ac.cn)

ABSTRACT Electronically tuned bandpass filters are crucial frequency-selective devices in tunable RF front-ends and are extensively utilized in the fields of communications and sensing. For low-cost and easy integration, varactor based tunable microstrip filters have been widely used in circuit design. The miniaturization, tuning flexibility, and performance optimization of tunable microstrip filters are all areas of concern. This paper reviews the research conducted on the varactor-diode-based tunable bandpass filters over the past decade. Numerous filters with various structures are introduced in the following sequence: frequency tuning, frequency and bandwidth tuning, transmission zero tuning, and tunable bandpass filter with special functions. The existing problems and limitations of various types of tuned filters have been discussed. The performance of several outstanding works has been analyzed and compared. Finally, the development direction of varactor-based microstrip tunable filters is objectively summarized, which will advance the research of microstrip filters.

INDEX TERMS Microwave circuit, microstrip filter, tunable bandpass filter, varactor diode, continuously tunable filter.

I. INTRODUCTION

In recent years, to meet the technical demands of wireless communications, radio frequency (RF) front-ends have been evolving to incorporate features such as multi-band, tunability, miniaturization, and low-cost, etc. [1], [2]. As a key frequency-selective component in the RF front-end, tunable filters expand the frequency range and reduce the complexity in multi-band communication systems. The performance of a tunable bandpass filter (TBPF) has attracted more attention.

Traditional cavity filters are known for their high-quality factor (Q), low noise, and low insertion loss (IL). However, they also have a larger footprint and limited reconfigurability, making them unsuitable for multi-band tunability [3], [4], [5]. On-chip filters offer the advantages of a small footprint and easy integration with the entire RF front-end, but their design flexibility is greatly limited by process [6], [7], [8]. In addition, their performances are relatively poor, and the cost will be higher. Microstrip filters are a popular choice because of their combination of performance, design flexibility, and ease of integration with other active elements. Especially the tunable filters with adjustable center frequency, bandwidth (BW), and transmission zero (TZ) tuning play an essential role due to their easy integration into wireless circuits and their ability to adapt well to various microwave systems.

A tunable microstrip BPF has been designed using various tuning components, such as varactors, MEMS, and p-i-n diodes, etc. [9], [10], [11], [12], [13], [14]. Among various tuning techniques, varactors are widely used because of their continuous tunability. In these studies, researchers

The associate editor coordinating the review of this manuscript and approving it for publication was Giorgio Montisci.

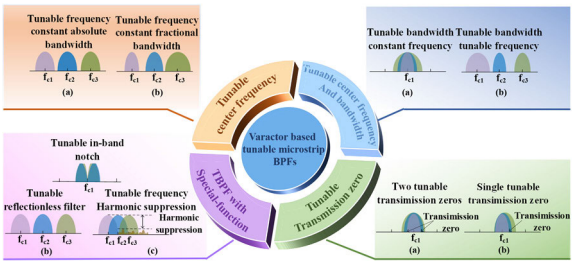

FIGURE 1. The sections and subcategories of the varactor based tunable microstrip bandpass filters.

have consistently focused on issues such as miniaturization, fewer tuning components [15], and easy-to-transplant design methods.

In this article, continuously tunable planar bandpass filters using varactor diodes are the main research subject. The discussion covered four types of tunable BPF including BPF with tunable frequency, BPF with tunable frequency and bandwidth, BPF with tunable transmission zero and TBPF with special-function. Each of the above types is further subdivided based on the main research direction. The sections and subcategories of the tunable filters discussed in this paper are shown in Fig.1. The performance of excellent works in each category was comprehensively compared such as frequency and bandwidth (BW) tunability, insertion loss (IL), and the number of control terminals. Finally, the development trends of the microstrip BPF based on varactor diodes were summarized, providing direction for future designs of continuously tunable planar.

II. BPF WITH TUNABLE FREQUENCY

Frequency tunability is one of the most crucial features of tunable filters. The operating frequency of a filter depends on the resonant frequency of a resonator. As a result, varactors are loaded at the resonator to control the operating frequency of the filter. There are many research focuses in this area, such as wider tuning range, multiple tunable passbands, and sharper frequency selectivity.

A. WIDE TUNABLE RANGE

The frequency tuning range of a varactor-based TBPF is primarily limited by the range of capacitance variation of the varactor (varactor ratio). Thus, the discussion of how to widen the tuning range only makes sense if the value of the varactor ratio is certain. In order to optimize the tuning range, researchers have proposed numerous structures and methods [16], [17]. The optimization approaches mainly include the following three types: switchable resonator, zero-value coupling technology, and resonator-based optimization.

Initially, switched filter banks are used to achieve wide-range tuning. In this way, the filter response provides good isolation between the different frequency bands. However, this solution tends to have a larger area. To address this issue, a switchable resonator structure was proposed innovatively. In [18], a tunable filter operating in the frequency range of 1.1-2.1GHz, which comprises two switchable resonators, was proposed. The structure is shown in Fig.2. By leveraging the principle that the resonant frequency can be controlled by the electrical length of a microstrip resonator, the filter's operating frequency switches between a lower frequency band and a higher frequency band when the p-i-n diode D_1 turns on and turn off. Multiple varactors are used to ensure a good response of the circuit during the tuning process. For example, varactor C_1 is utilized to achieve continuous frequency tuning of the filter in every mode. C_2, C_3, and C_4 are used to adjust the coupling coefficient and external Q value, respectively. It should be noted that since C_2 and C_3 are loaded in the middle of the resonator, their position and value will affect the resonant frequency (according to the odd-even mode analysis). Since the structure incorporates a relatively large number of switching diodes and varactors, the insertion loss of the filter is poor, which is also evidenced by the measured results in Fig.3. The insertion loss is 4.4-6.1dB in the entire tuning range.

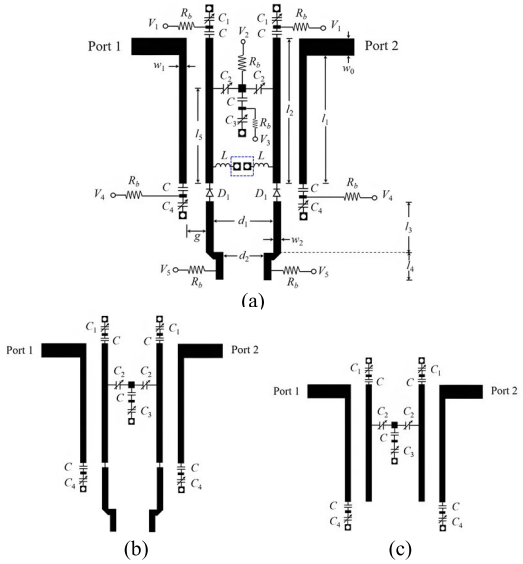

FIGURE 2. (a) Structure of the BPF with switchable resonator. (b) Lower frequency mode (c) Higher frequency mode [18].

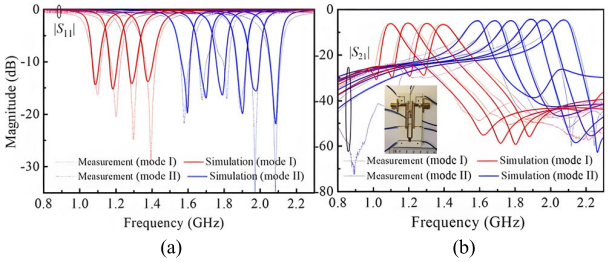

FIGURE 3. Measured and simulated results of (a) S_{11} and (b) S_{21} [18].

The filter in Fig.4 follows the same idea, but differs in that its inter-stage coupling coefficient cannot be tuned in a single mode [19]. Reduced tuning devices improve IL. The

measured S-parameters of the two modes are shown in Fig.5. The tuning range of the BPF is 0.55-1.99 GHz. The measured IL is 3.3-4.4 dB. In this study, the structure is extended to a higher order to enhance the filter roll-off.

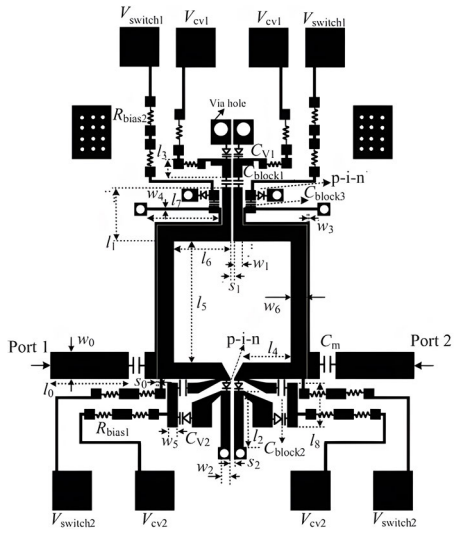

FIGURE 4. Diagram of the proposed two-pole filter in [19].

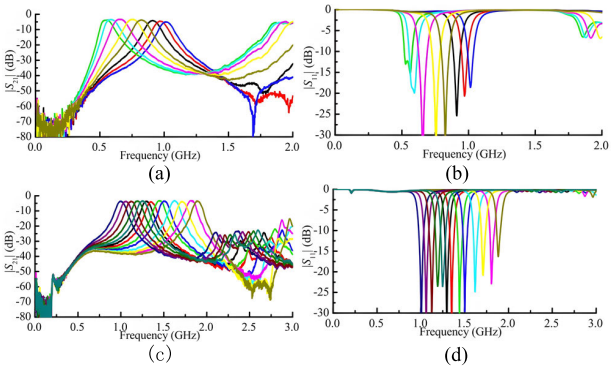

FIGURE 5. Measured results of (a)S_{21} and (b)S_{11} in lower band and(c) S_{21} and (d)S_{11} in higher band [19].

Even though the above method expands the frequency tuning range and effectively reduces the circuit area, the low Q value of the p-i-n diode still degrades the IL of the filter. Zero-value coupling technology achieves the switching function by adjusting the coupling coefficient without the need for additional switches, effectively avoiding this issue. In [20], dual zero-value coupling resonators were used to create two different operating bands in order to widen the tuning range. Fig.6 (a) shows the two-pole filter. Coupled-line A and B generate the low-band and high-band signals, respectively. The electric varactors C_{v12L} and C_{v12H} are utilized to cancel the magnetic coupling from the coupled-line A and B in order to achieve zero-value couplings, resulting in the corresponding frequency band being turned off. Frequency tuning within each band is controlled by varactors C_{v1L} and C_{v1H}. Fig.6(b) displays the tuning results of the fabricated 2-pole filter. The tuning range is 0.75-1.09 GHz and 1.70-2.18 GHz. Another 4-pole filter has resonant frequencies that are closer together in the high and low bands, allowing for continuous wide tuning. Its structure and measured S_{21} are shown in Fig 7. It also demonstrates improved frequency selectivity.

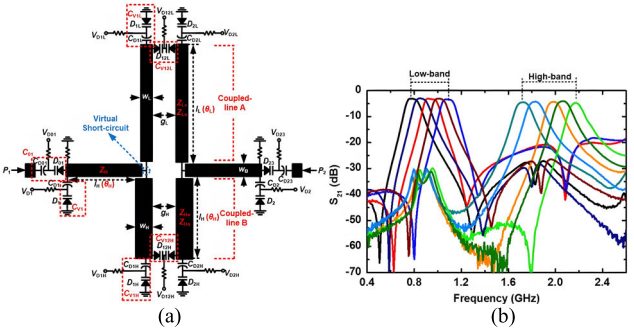

FIGURE 6. 2-pole filter (a) Layout (b) Measured S_{21} of fabricated filter in [20].

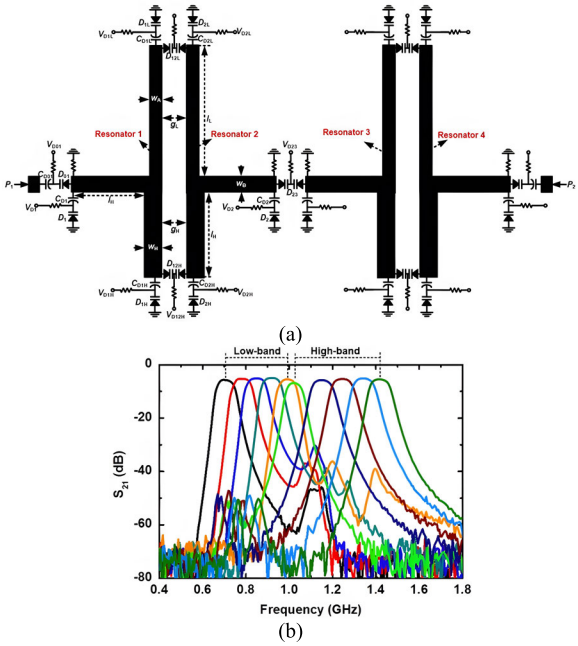

FIGURE 7. 4-pole filter (a) Layout (b) Measured S_{21} of fabricated filter in [20].

Optimizing the resonator to extend the tuning range is a more fundamental approach. In 2015, Jian-Xin Chen et al. designed a new capacitor-loaded stepped-impedance resonator (SIR). As shown in Fig.8(a) [21]. Capacitors C_{v1} and C_{v2} are loaded at the open ends and the center of the SIR, respectively. In the traditional capacitor loading method, the resonant frequency of the resonator moves to a lower frequency as the capacitance varies. This new loading method enables the even-mode resonant frequency to shift to a higher or lower frequency by controlling the values of C_{v1} and C_{v2}. The bidirectional tuning method doubles the range of tuning.

Fig.8(b) shows the layout of the designed TBPF. The signal feed line is connected to the center of the SIR to effectively suppress the odd-mode resonant frequency. The tuning range of this structure reaches 84.4%, with an insertion loss of 1-3.1dB across the 0.77-1.42 GHz, as shown in Fig.9.

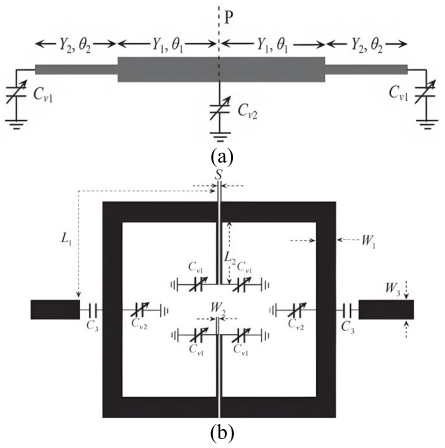

FIGURE 8. The (a) structure of bidirectionally tunable resonator and (b)layout of proposed tunable BPF in [21].

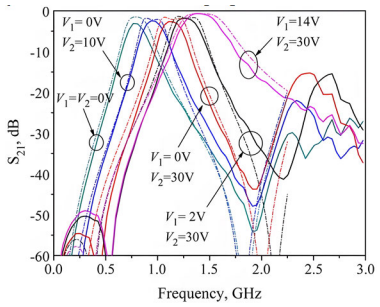

FIGURE 9. Measured S_{21} of the fabricated tunable filter in [21].

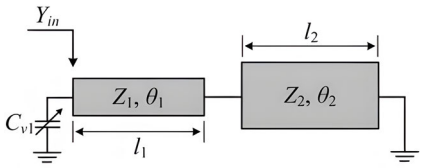

FIGURE 10. The varactor-loaded λ/4 SIR in [22].

In 2017, the same research team reported further advancements in the SIR. The researchers discovered that there is an optimal length ratio of the loaded SIR to achieve the largest frequency tuning range [22]. Theoretical analysis of the quarter-wavelength resonator, as depicted in Fig.10, revealed that a length ratio u (u=l1/(l1+l2)) is near 0.6, the tuning range can be obtained the maximum value whatever the value of the characteristic impedances of the SIR. As shown in Fig.11. Based on this finding, a TBPF is demonstrated as shown in Fig.12(a). An appropriate coupling region must be selected to ensure that the filter's fractional bandwidth remains as constant as possible during the tuning process. C_{v2} is located at the feed line to tune external Q. Fig.12(b) presents the measured results. The fabricated filter achieves a tuning range of 0.6-1.015GHz.

Table 1 shows a performance comparison of the frequency-adjustable filter. Circuits that incorporate switches will expand the tuning range [18], [19], [20], but they may also result in a 1-2dB increase in insertion loss. Optimizing the resonator can expand the tuning range without increasing the insertion loss [21], but there are limitations to extending the tuning range in this manner.

B. DUAL-BAND TUNABILITY

Dual passband adjustable filters comprise single passband adjustable filters and double passband adjustable filters [23], [24], [25]. In any case, the essence of the research lies in extracting independent adjustable methods from the structure and reducing the design complexity of the control circuit.

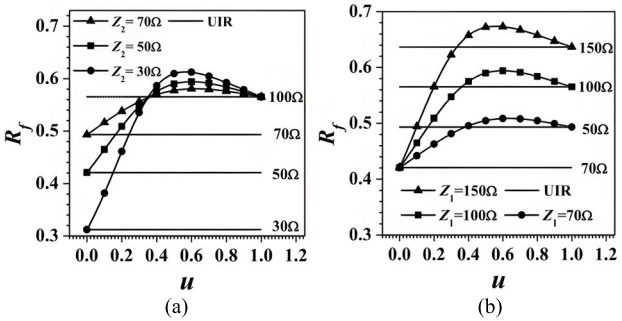

FIGURE 11. Simulated Rf with different u and Z_i (i=1 or 2). (a) Z_1 =100Ω(b) Z_2 =50Ω.Rf is the tuning range (R_f =(f_{0h}-f_{0l})/((f_{0h}+f_{0l})/2)) [22].

TABLE 1. Performance comparison of the BPF with wide frequency tuning range.

Refs	Frequency Tuning range (GHz)	Number of tuning elements	3-dB BW (MHz)	IL(dB)	Size (λ_g^2)
[17]	1.1-1.88	3	90±8	6.8-4.3	0.20×0.18
[18]	1.1-2.1	9	40	4.4-6.1	0.06×0.27
[19]	0.55-1.9	6	92±6	3.2-4.4	0.14×0.19
	0.54-1.8	12	89±4	4.0-5.4	0.14×0.23
[20]	0.7-1.44	24	61±6	6.1-6.5	-
[21]	0.7-1.42	6	176±88	3.1-1.0	-
[22]	0.6-1.015	4	124±2	1.1-2.8	0.19×0.19

*λ_g: guided wavelength at the center of frequency tuning range.

To independently adjust a single frequency band in a dual-band filter, it is essential to identify structural factors that can independently influence the single frequency band. In [26], a differential dual-band tunable BPF was demonstrated. The filter consists of two SIRs, a pair of loaded tunable varactors, and a centrally loaded resistor. As shown in Fig.13. Resistor R is used to suppress the even-mode resonant frequency. The double passband results from the resonant frequencies of the odd mode. The varactor C2 is loaded at a specific

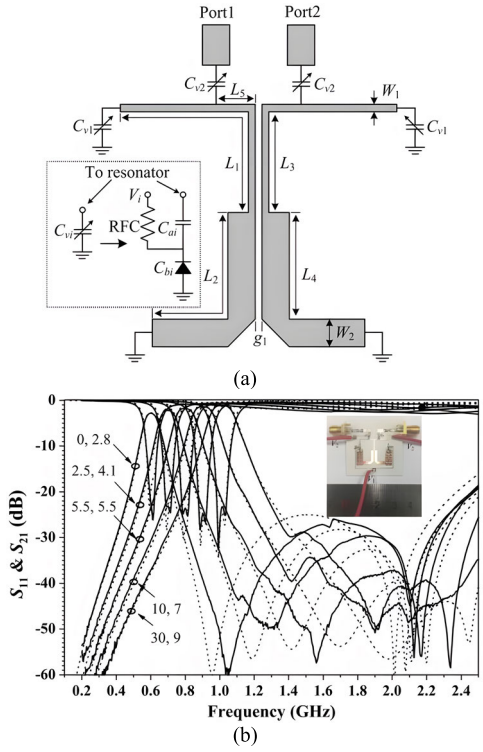

FIGURE 12. (a) Schematic and (b) measured results of the proposed TBPF in [22].

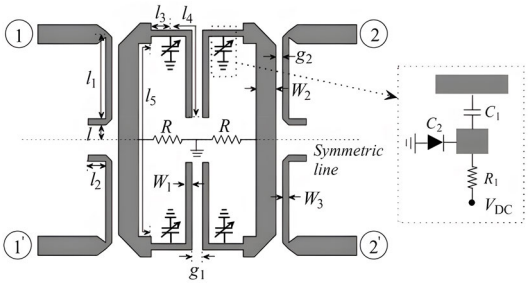

FIGURE 13. Structure of tunable differential filter in [26].

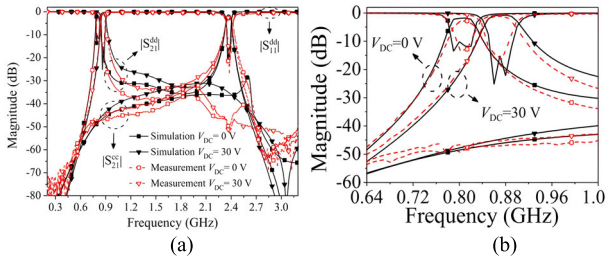

FIGURE 14. Simulated and measured S-parameters. (a) Overall band (b) Lower band [26].

location, and its adjustments will have minimal impact on the high- frequency band, allowing for independently tunable frequencies. Two SIRs are coupled through a slit in the middle.Fig.14 shows the tuning results. The lower band can be tuned while the upper one remains fixed.

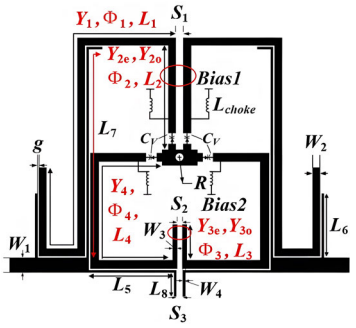

FIGURE 15. Structure of proposed dual-band tunable filter in [27].

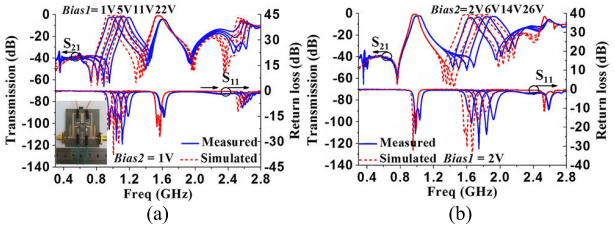

FIGURE 16. Measurement and simulation of fabricated filter. (a) lower band tuning (b) higher band tuning [27].

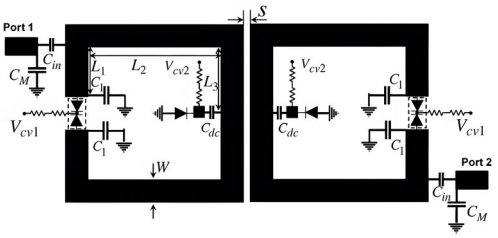

FIGURE 17. Structure of proposed two-port filter in [28].

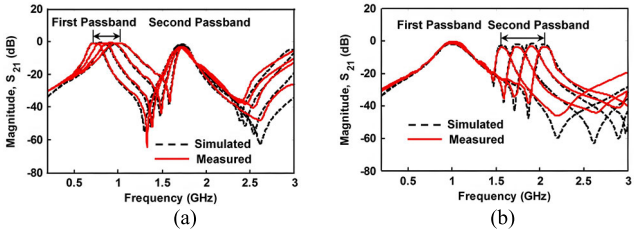

FIGURE 18. Measured and simulated S_{21}. (a) Variable lower frequency band (b) Variable higher frequency band [28].

Fig.15 shows a dual-band BPF with independently tunable passbands [27]. Bias 1 controls a pair of λ/4 resonators loaded with varactors to form the first band, while bias 2 controls the second one. The coupling between the two passbands in this structure is very weak (relatively far physical distance), so the passbands do not affect each other. Fig.16 shows the measurement and simulation of the fabricated filter. The tunable frequency ranges of the passbands are 0.98-1.22 GHz and 1.63-1.95 GHz, respectively.

There is no doubt that the above method of weakening the influence between two passbands through physical distance increases the circuit area. Another method involves using different modes of the same resonator to generate

TABLE 2. Comparison of dual-band tunable filters.

Refs	Frequency tuning range (GHz)		Bandwidth (MHz)		IL (dB)	Number of tuning elements	Size (λ_g^2)
	Frequency1	Frequency2	BW1	BW2			
[23]	1.48-1.29	3.65	79-76	234	1.45-4.21	4	-
[25]	0.88-1.08	1.68-1.85	60±4	70±5	1.4-6.9	4	0.19×0.47
[26]	0.87-0.81	2.4	42	72	<2.8	4	-
[27]	0.98-1.22	1.63-1.95	76±4	100±4	2.1-4.0	4	0.21×0.17
[28]	0.77-1.02	1.57-2.0	200±21	120±8	0.7-3.9	4	-

*λ_g: guided wavelength at the center of frequency tuning range.

two passbands. As shown in Fig.17, the proposed TBPF consists of two coupled split-ring resonators loaded with varactors [28]. The first band is formed by the odd-mode resonator, and its center frequency depends on the varactors loaded at the split of the ring. The second band is formed by the even-mode resonator, which can be tuned by loading a varactor at the center of the transmission line. Thus, the proposed filter achieves dual-band frequency-independent tuning. Fig.18 shows measured and simulated S_{21} with varying frequencies. The frequency tuning range is 0.77-1.02 GHz and 1.57-2.0 GHz.

Table 2 presents several comparisons of dual-band tunable filters. Compared to single-band adjustable filters, the overall performance of dual-band filter tuning is inferior. Independent control technologies for individual frequency bands in tuning still need to be explored.

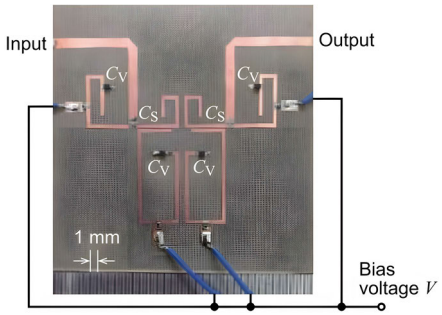

FIGURE 19. Photograph of fabricated 4th-order BPF in [29].

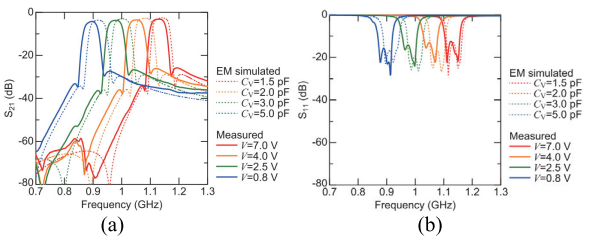

FIGURE 20. Measurement and EM simulation of (a) S_{21} and (b) S_{11} [29].

C. HIGH SELECTIVITY

There are two ways to enhance the selectivity of filters. One option is a cascade multi-stage filter, which features a simpler tuning mechanism but requires a larger circuit area. The other purpose is to introduce transmission zeros. Adaptive transmission zeros help the filter maintain good selectivity. This method could reduce the area, but its tuning mechanism is relatively more complex. In addition, frequency-tunable filters must also consider how the coupling coefficient and external Q value maintain the expected changing relationship during the frequency tuning process in order to achieve the best frequency response.

The authors of [29] fabricated a 4th-order and a 6th-order microstrip tunable BPFs that exhibited excellent roll-off characteristics. Fig.19 shows the structure of a 4th-order filter. The C_V loaded on four resonators controls frequency tuning. This proposed structure effectively utilizes the intrinsic frequency dependence of inter-resonator couplings to minimize the number of tuning components. This approach achieves a constant absolute bandwidth (ABW) through a straightforward dc-bias control. Fig.20 shows the measured S-parameters with variable frequency. Higher order filters have high selectivity, and it is possible to specify zeros on both sides of the band in advance. The frequency tuning range is 0.89-1.13 GHz.

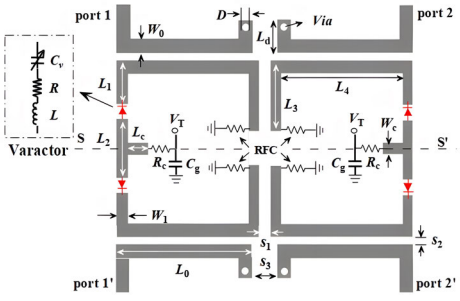

FIGURE 21. Layout of balanced TBPF in [30].

In [30], a balanced TBPF consisting of two open-loop resonators loading a pair of varactors was proposed. As shown in Fig.21, a pair of varactors (C_V) are loaded at a specific position to tune the desired frequency range. The stub and R_c are loaded to suppress the even mode resonant frequency to optimize frequency response. The source-load coupling between four coupled feed lines creates two frequency-dependent transmission zeros on both sides of the

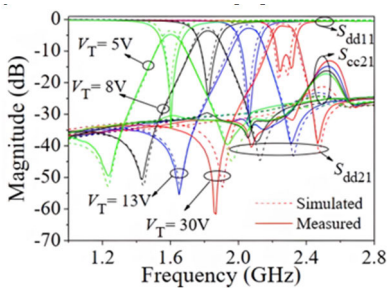

FIGURE 22. Simulated and measured results of proposed filter in [30].

passband. Adaptive transmission zeros maintain the filter's frequency selectivity during variable frequencies. As can be seen in Fig.22. The center frequency of the fabricated filter can be tuned from 1.6 to 2.27 GHz. The common-mode (CM) suppression exceeds 30dB.

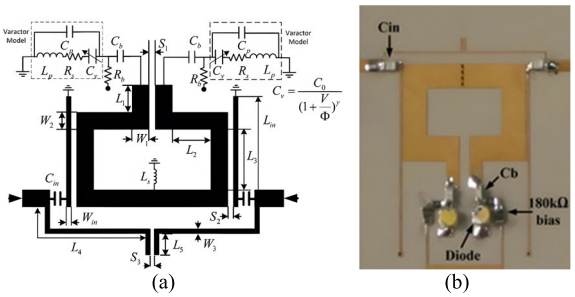

FIGURE 23. (a) Structure and (b) photograph of designed filter in [31].

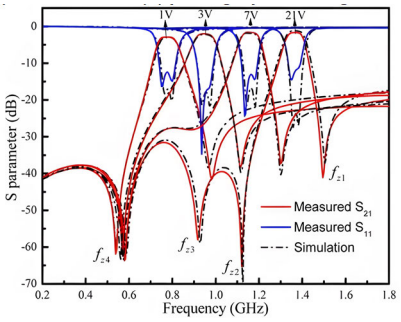

FIGURE 24. Measurement and simulation of tunable filter in [31].

A two-path mixed coupling filter with high selectivity was fabricated in [31], which designed an additional resonance circuit to generate tunable transmission zeros. As shown in Fig.23, two transmission zeros can be adjusted by the source-load coupling (fixed Cin and a shorted microstrip line). Two additional transmission zeros are generated by an input network, which could be adjusted via L5. In addition, two transmission lines are coupled at one end where the varactors are loaded (the first coupling path: electric coupling), and at the other end they are coupled by semi-lumped through-via (the second coupling path: magnetic coupling). The mixed coupling method can flexibly adjust the coupling coefficient to achieve a wide range of tuning. Fig.24 shows the measured response at various frequencies. The center frequency tuning range is 0.78-1.36 GHz. In the same year, the literature [32] embraced a similar concept to develop a highly selective dual-band filter using source-load coupling and T-shape stub-loaded lines. The proposed filter has 5-6 transmission zeros across the entire frequency range and provides greater than30dB rejection between two bands.

TABLE 3. Comparison with different tunable high selectivity filters.

Refs	Frequency Tuning range (GHz)	Filter order	Insertion loss (dB)	Number of TZs
[29]	0.89-1.13	4	3.2-4.3	2
[30]	1.60-2.27	2	4.17-1.99	2
[31]	0.78-1.36	2	1.68-2.9	4
[32]	0.8-1.02	2	1.12-2.93	6
	2.02-2.48		1.45-4.89	

Table 3 shows a performance comparison of previously reported excellent works. At present, the selection performance of tunable filters in the tuning process is not fully discussed, such as the roll-off factor, suppression level, and the range of suppression in both lower and upper stop bands. The focus remains on tuning range and insertion loss.

III. BPF WITH TUNABLE FREQUENCY AND BANDWITH

Frequency tuning primarily depends on the resonant frequency, while bandwidth tuning primarily depends on the coupling coefficient. One way to adjust bandwidth is by modifying coupling, which includes interstage coupling and input-output coupling [33] [34]. Therefore, in theory, more bias terminals are needed to simultaneously tune frequency and bandwidth.

In order to simplify the control of inter-resonators, cross-shaped multi-mode resonators are represented in [35] to achieve a tunable bandpass filter. Measurements show that the center frequency of the fabricated filter can be tuned from 600 to 1450 MHz. The return loss is more than 15dB and the insertion loss is less than 4dB over tuning range. The bandwidth can vary from 120 to 950 MHz when the center frequency is 1 GHz.

The authors in [36] proposed a design theory for a dual-mode BPF with an element-variable coupling matrix. The proposed coupling matrix can predict the frequency response of the filter. By varying the variable elements of the coupling matrix, both the frequency and bandwidth of the filter can be tuned. Fig.25 shows the structure of the proposed filter. The center frequency and bandwidth of the filter will be tuned by varactors C_{de} and C_{dm}. The measured tuning results are shown in Fig.26. The filter maintains a good passband shape during frequency tuning.

Qing-Xin Chu et al. proposed a novel multi-mode resonator whose differential-mode resonant frequency is tuned by the loaded varactors, while the varactors have a negligible effect on the common-mode frequency response.

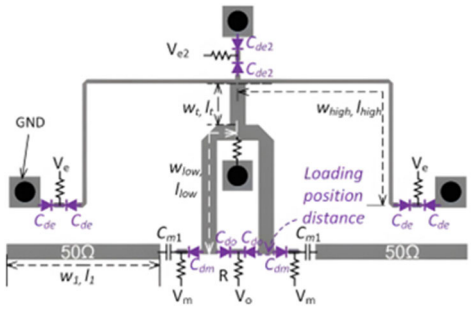

FIGURE 25. Schematic of the dual-mode filter in [36].

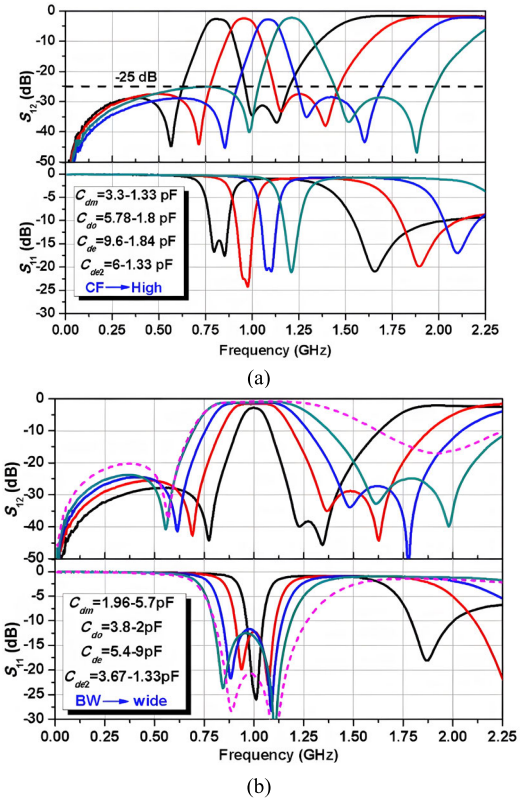

FIGURE 26. Measurement of fabricated fully tunable filter. (a) frequency tuning (b) bandwidth tuning [36].

The structure of the resonator is shown in fig.27(a) [37]. In differential mode response, the even-mode resonance frequency can be independently tuned with C_{V2}, and the frequency of the odd mode remains constant. This property makes it possible to tune the filter bandwidth. In addition, by selecting a suitable microstrip line lengths L_1 and L_2, the common-mode resonance frequency could be suppressed at a higher frequency without adding any circuit elements. The balanced filter structure based on this resonator is shown in fig.27(b). The capacitor C_s is used to adjust the external Q. Fig.28 shows the measured results of frequency tuning and bandwidth tuning. The measured center frequency tuning range is 0.8-1.52 GHz. The common mode is effectively suppressed across the tuning range.

Another way to implement a BPF with tunable bandpass and frequency is to cascade two filter units with different frequency responses. In [38], a BPF with an adjustable passband edge was designed by directly cascading a high-pass filter (HPF) and a low-pass filter (LPF). Fig.29 shows the layout of the proposed filter. HPF is on the left, and LPF is on the right. The passband edges (cutoff frequencies) of LPF and HPF are controlled by loaded varactors. This structure eliminates the frequency-dependent limitations of coupling coefficients and external Q values during the tuning process, resulting in a simpler design process. Fig.30 and Fig.31 show the measurements of frequency tuning and bandwidth tuning of the filter. It can be seen the fabricated filter exhibits a sharp roll-off and maintains a good in-band shape within the tuning process of frequency 0.8-1.95 GHz and bandwidth of 180-1390 MHz.

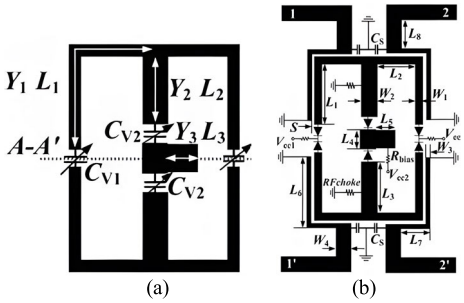

FIGURE 27. Layout of proposed (a) multi-mode resonator and (b) balanced BPF in [37].

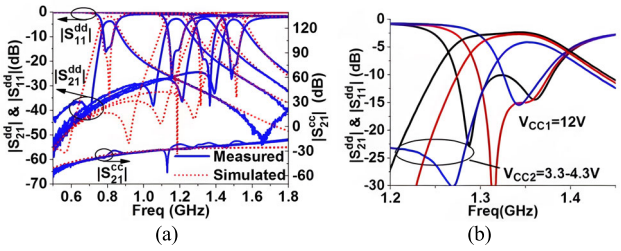

FIGURE 28. Measurement and simulation S-parameter of fabricated BPF. (a) Frequency tuning. (b) Measured frequency responds with bandwidth tuning [37].

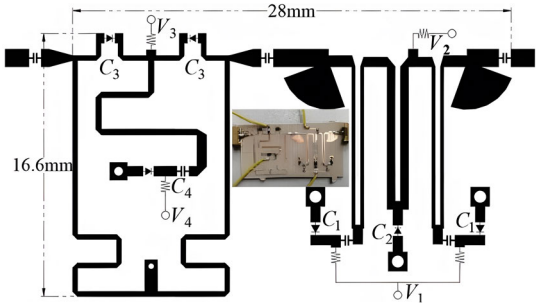

FIGURE 29. Layout and fabrication of HPF-LPF cascade filter in [38].

Table 4 presents a performance comparison of several previously reported excellent works. BPFs with tunable

TABLE 4. Comparison of several reported BPF with tunable frequency and bandwidth.

refs	Frequency tuning range (GHz)	Bandwidth tuning range (MHz)	Insertion loss (dB)	Number of components	Size (λ_g^2)
[33]	0.58-1.22	65-180	1.8-4.6	12	0.12×0.08
[34]	0.59-0.88	115-315	1.19-1.53	7	-
[35]	0.7-1.22	140-644	1-2	6	-
[36]	0.8-1.42	50-500	≤3.8	10	-
[37]	0.8-1.52	63-140	2.4-5.8	4	0.11×0.08
[38]	0.8-1.95	180-1390	1.3-5.2	4	0.027

*λ_g: guided wavelength at the center of frequency tuning range.

frequency and bandwidth typically require more control components. The increased control ports also ensure a good response across the entire tuning range. The structure of HPF cascaded LPF can achieve a wider frequency and bandwidth tuning range, but it also occupies a larger area.

IV. BPF WITH TUNABLE TRANSMISSION ZERO

As previously mentioned, the introduction of transmission zeros into the bandpass filter can improve out-of-band suppression and enhance frequency selectivity. However, these zeros cannot be adjusted flexibly. In recent years, a variety of transmission zero tuning mechanisms have been proposed [39], [40], [41]. In [39], Bin-Feng Zong et al. designed a BPF with two tunable transmission zeros close to the passband by adjusting the ratio of electrical and magnetic coupling. In [40], a stub loaded with a varactor diode was introduced between two parallel coupled lines to control the TZ near the lower or higher band edges.

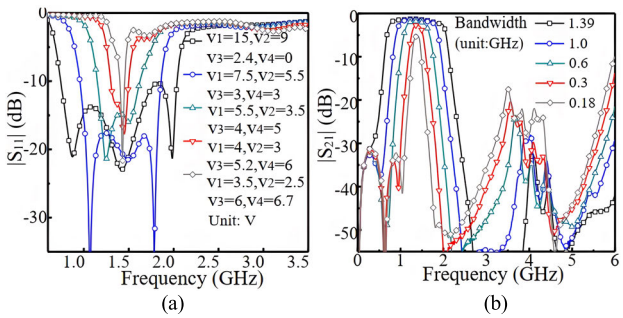

FIGURE 30. Measured (a) S_{11} and (b) S_{21} with variable bandwidth (center frequency is 1.4GHz) [38].

The main concepts of these tuning mechanisms are categorized into two groups. The first method is to use the band-pass and band-resistance cascade technique to improve the suppression of specific frequency points and dynamically control the notch frequency. This approach offers greater flexibility. However, compared to other filters of the same order, cascaded filters have a poor roll-off near the passband and typically experience increased mismatch losses during tuning. The second is to adjust the coupling mechanism to control the transmission zero. This method has a simpler structure but is limited by bandwidth, frequency, etc.

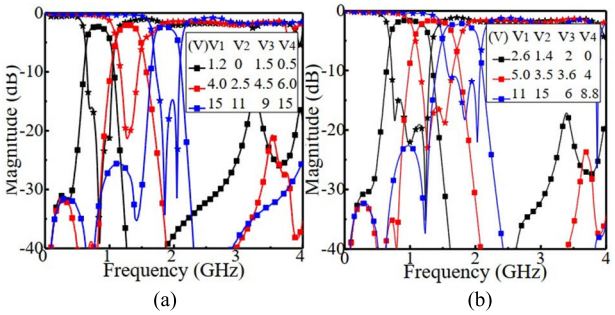

FIGURE 31. Measured response of variable frequency (a) ABW=400MHz, (b) ABW=600MHz [38].

A filter employing bandpass-bandstop filter cascade was demonstrated in [42]. This filter dynamically controls TZs close to passband and achieves excellent selectivity without any additional mismatch loss. The proposed filter is shown in Fig. 32. Butterworth BPF considering impedance mismatch and bandstop (BSF) with controllable phase provide maximum flexibility in tuning frequency, bandwidth, and TZs. Fig.33 shows measured frequency response with variable transmission zeros at two central frequencies. The black, olive, and blue lines represent the FBWs of 9%, 6%, and 3%, respectively. In all cases, the return loss is greater than 15dB.

In [43], a two-pole BPF with tunable combline filter was developed, which generates tunable transmission zeros through source-load coupling. As shown in Fig.34, varactors loaded at the end of microstrip lines are designed to control frequency tuning. The T-type network connected between resonators was used to adjust the coupling coefficient. The tuning of TZs is controlled by back-to-back varactors C_4. Fig.35 shows the measured S_{21} of the fabricated filter when TZs tune from 300 to 700 MHz.

In [44], a constant absolute bandwidth filter with tunable TZs was proposed, which consists of asymmetrical spiral resonators and loaded varactors. The number and location of transmission zeros are related to the values of loaded varactors. The proposed filter is shown in Fig.36. Coupling varactor between the two resonators D_2 can change the response from two TZs to zero TZ. Varactors D_3 loaded at the input/output circuit are used to control the response that having TZs either on one side or both sides of the passband.

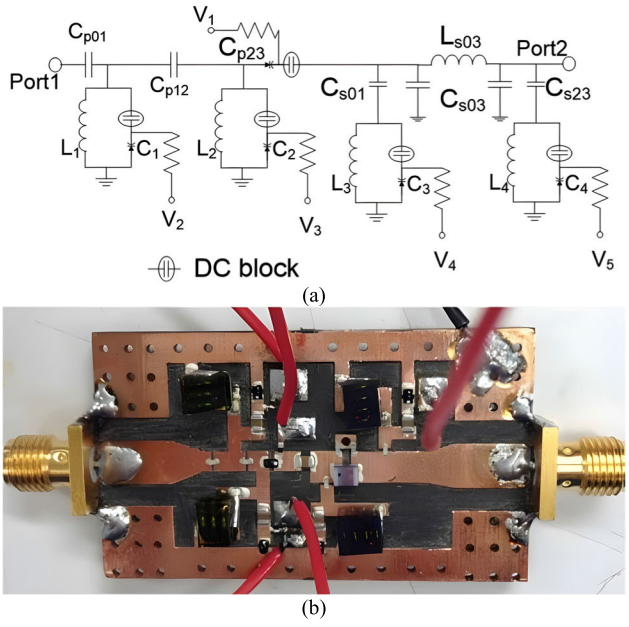

FIGURE 32. (a) Schematic and (b) photograph of fabricated filter in [42].

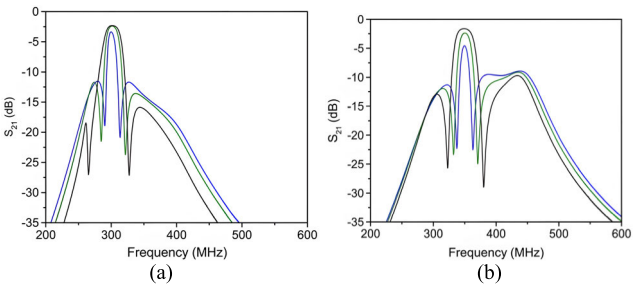

FIGURE 33. Measured frequency response with variable TZs (a) Center frequency is 300MHz (b) Center frequency is 350MHz [42].

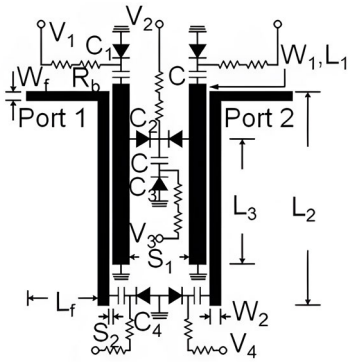

FIGURE 34. Configuration of the proposed combline filter in [43].

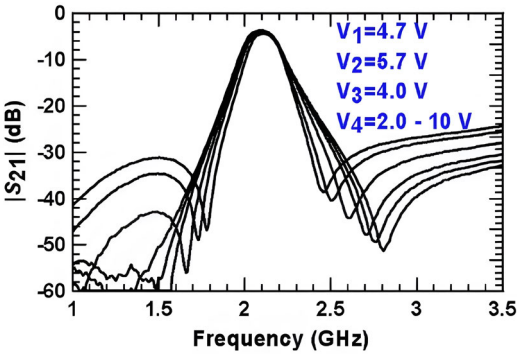

FIGURE 35. Measured S21 of proposed filter with TZs tuning from 300 to 700MHz [43].

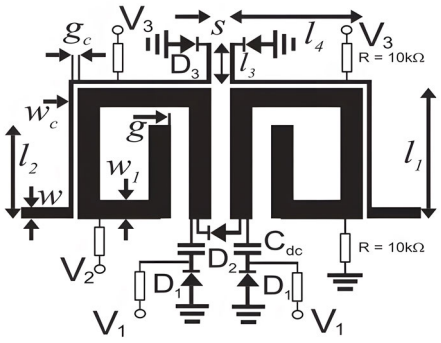

FIGURE 36. Layout of the proposed filter with reconfigurable TZs [44].

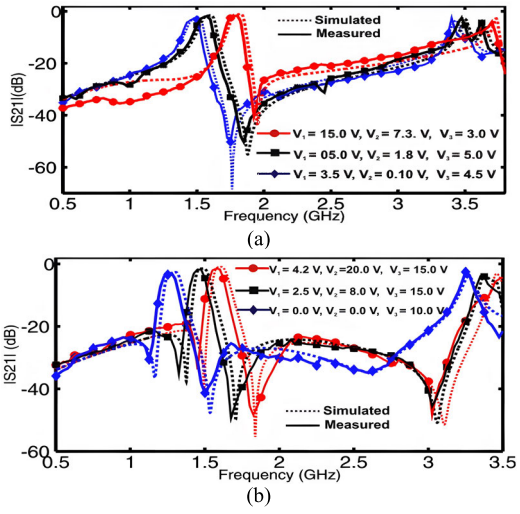

FIGURE 37. Measurement and simulation of BPF with tunable TZs on (a) higher side and (b) both sides [44].

Fig.37 shows the measured S_{21} of a manufactured BPF with tunable TZs.

The suppression could be optimized by adjusting TZs appropriately.

Table 5 presents various filter structures with tunable transmission zeros. The impact of tunable transmission zeros on filter response varies; some varies the absolute bandwidth, while others adjust the frequency. In either case, the main purpose of introducing zero points is to improve selectivity.

V. TBPF WITH SPECIAL-FUNCTION

In addition to the general tuning objectives mentioned above, tunable filters also have some special functions that need to be focused on, mainly including tunable in-band notch, tunable

TABLE 5. Comparison of BPFs with tunable transmission zeros.

Refs	Center frequency (GHz)	Band width (MHz)	Insertion loss (dB)	Number of TZs
[40]	0.95-1.45	80-100	<3	1
[41]	0.75-1.24	55-175	>0.5	-
[43]	1.7-2.7	50-110	4.9-3.8	2
[44]	1.47-1.8	105	2.8-1.3	1
	1.27-1.6	92	3.4-1.5	2

reflectionless filters, and harmonic suppression during tuning process.

A. TUNABLE IN-BAND NOTCH FILTER

In ultra-wideband (UWB) systems, many narrowband interference signals affect the information reception. Therefore, notch filters are needed to protect the system from undesired interference. Notch bandpass filters that combine preselection and interference suppress are multi-functional filters. Existing notch design solutions mainly involve the use of additional notch resonators [45], embedded open stubs [46], and asymmetric coupled feeders [47]. To suppress in-band interference dynamically, notch tunable filters are required [48], [49], [50]. Recently, Reconfigurable notch BPFs with tunable bandwidth have also been reported [51], [52], [53].

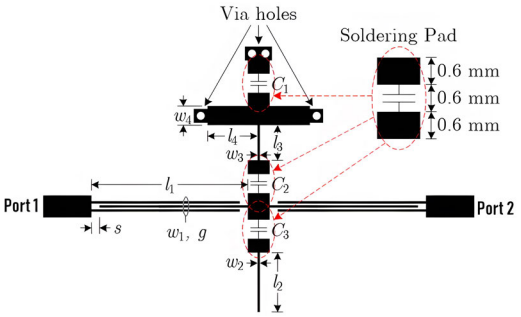

FIGURE 38. Structure of the proposed BPF in [51].

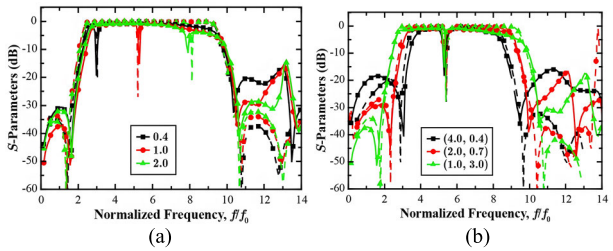

FIGURE 39. Measurement (solid lines) and simulation (dash lines) of S-parameters with (a) Tunable notch frequency (variable C_1) and (b) tunable bandwidth (variable C_2) in [51].

In [51], a notch tunable BPF based on dual cross-shaped resonator (DCSR) was demonstrated as shown in Fig.38. DCSR is a further structure of CSR. A new sub-branch of stubs extends from the end of the parental stub. Varactor C1-3 can be used to adjust filter frequency response. In this work, filters with different tuned objects are fabricated. The measured results are shown in Fig.39. The notch frequency tuning range is 3-7.9 GHz. The bandwidth tuning can be tuned from 5 to 7.5 GHz when the notch is fixed at 5.3 GHz.

Table 6 shows different tunable in-band notch filters. Notch filters are mainly used in broadband systems. The introduction of the notch structure will not affect the performance of the filter passband itself. The main problem is how to maintain better suppression during notch-band tuning.

TABLE 6. Comparison with different tunable in-band notch filters.

Refs	Center frequency (GHz)	Band width (MHz)	Notched-band tuning	Notch-band rejection (dB)	Circuit size (λ_g^2)
[49]	6.8	5576	4.6-6.5	>15	0.47× 0.22
[51]	6	4980-7260	3.0-7.9	>15	-
[52]	0.9	400	0.7-1.1	>17	-
[53]	2	-	1.81-1.97	>17	-

*λ_g: guided wavelength at the center of frequency tuning range.

B. TUNABLE REFLECTIONLESS FILTER

The out-of-band signal reflection of a filter will affect the performance of the active units in RF front-end. Different from the traditional reflective filters, reflectionless filters Dissipate the energy of the OOB signal inside, which not only omit the interstage isolator [54], but also relive the pressure of the linearity of the front stage circuit. Based on the design of frequency-static reflectionless BPF, a tunable reflectionless filter mainly solves the problem of reflectionless mechanism synchronization during frequency tuning [55], [56].

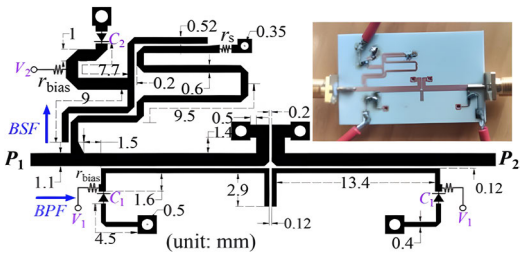

FIGURE 40. Layout and photograph of designed reflectionless filter in [57].

In [57], a frequency tunable input-reflectionless BPF with constant bandwidth was reported. It is composed of a main channel and an auxiliary channel, which are configured synchronously in a wide frequency range. The main channel is used to transmit in-band signals to the output port, and the auxiliary channel load resistance is used to dissipate the out-of-band signals reflected back by the main channel. To achieve a frequency tunable reflectionless filter, the

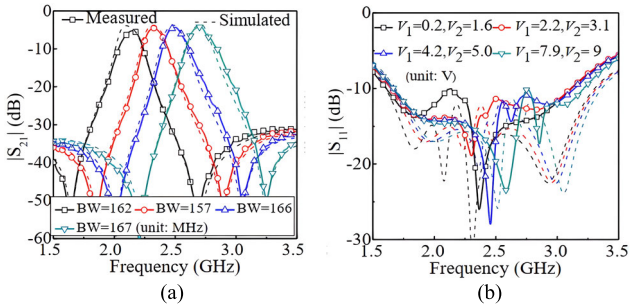

FIGURE 41. Measured and simulated results of fabricated filter (a) S_{21} (b) S_{11} [57].

center frequencies of the two channels must be tuned synchronously.Fig.40 shows proposed structure.

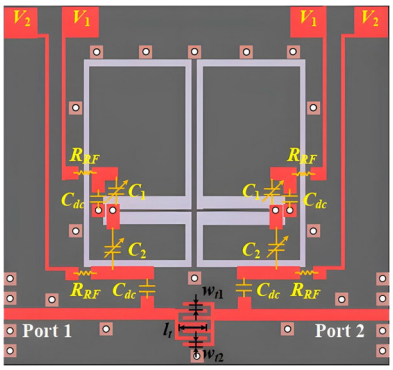

FIGURE 42. Configuration of proposed filter in [61].

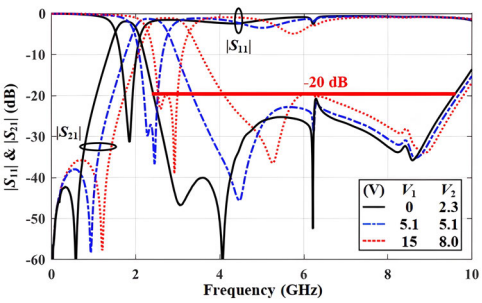

FIGURE 43. Measured S-parameter of fabricated filter with wide stopband in [61].

The main channel is made up of quarter-wavelength resonators loaded varactors and parallel-coupled lines. The auxiliary channel is designed using a dual-mode resonator. Fig.41 shows measured S-parameter of frequency tuning (2.11 GHz-2.72 GHz). The OOB input reflection is lower than -10dB.

In the same year, the same researcher proposed a dual-band tunable reflectionless filter using balanced circuit with two reflective-type BPFs [58]. The reflected stopband signal in dual-path is eliminated at the input end. Authors of [59] proposed another method to implement an independently tunable dual-band reflectionless filter. The dual band is generated by only one multi-mode resonator, and the reflection absorptivity is achieved by an absorptive network.

C. HARMONIC SUPPRESSION

The harmonic inherent in a tunable filter leads to relatively poor stopband suppression during frequency tuning. Harmonic suppression is one of the key problems of tunable filters. One way to suppress harmonic is inserting a TZ at harmonic frequency. But this method will be inefficient when tuning range is wide [60]. Another way is Defected Ground Structure (DGS). Many designs achieved harmonic suppression in a wide range because its band-rejection characteristics [61], [62], [63].

To create a wide stopband, a varactor-diode controlled filter based on substrate-integrated defected ground structure (SIDGS) resonator was demonstrated [61]. SIDGS is a technology that helps obtain higher inductance so that the proposed filter achieves harmonic suppression in a wider band. Fig.42 shows the configuration of proposed filter.

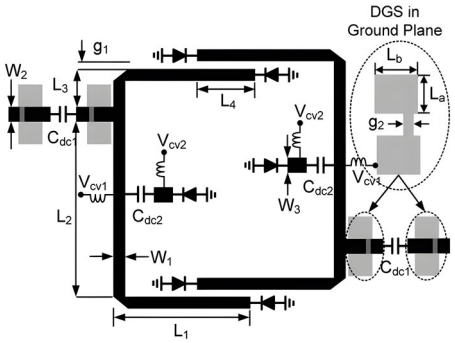

FIGURE 44. Schematic of proposed dual-band filter in [62].

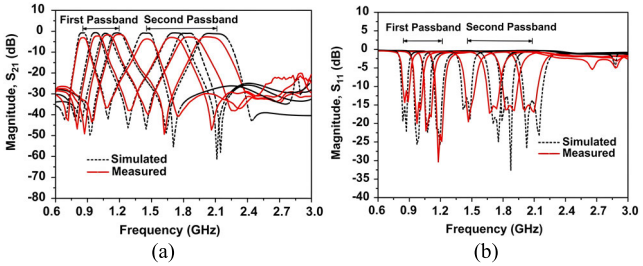

FIGURE 45. Measured and simulated S-parameter with variable frequency. (a) S_{21} (b) S_{11} [62].

Varactor diodes are cascaded behind half-wavelength resonators. The fundamental frequency can be tuned by varactors while the first harmonic is maintained at higher frequency. Fig.43 shows measured S-parameter. As can be seen, the stopband suppression is better than 20dB for the entire frequency tuning range (1.75-2.7 GHz). The return loss is also lower than -20 dB.

Similarly, a dual-band BPF using DGS on input/output feed lines achieved excellent harmonic suppress [62]. As shown in Fig.44. Two microstrip resonators loaded

varactor diodes are used to generate two tunable passbands. DGS that used at input/output offers not only has band-rejection characteristics at a specific frequency but also provide extra effective inductance of transmission line. Measured harmonic suppression is better than 20 dB up to 18 GHz. The frequency tuning range of two band is 0.85-1.2 GHz and 1.4-2.14 GHz, respectively. (As shown in Fig.45.).

VI. SUMMARY AND PROSPECT

Tunable microstrip filters have better frequency response due to the flexibility in board material selection and graphic design. Currently, there have been many excellent designs in terms of frequency tuning, bandwidth tuning, and TZs tuning. These designs include discussions on many issues such as tuning range expansion, independently adjustable tuning targets, dual-band tuning, common mode suppression, harmonic suppression, and reflectionless filters, etc. In each solution, miniaturization, fewer tuning components, lower losses, and higher performance have always been the goals pursued by designers.

In addition to the exploration of various new tunable filter structures, new design methods and theoretical systems are also constantly being proposed, but this part of the work is relatively less and lacks universality. The simplification of the tuning circuit and the scalability of a design method are also the focus of tunable filter research.

Moreover, varactor-based continuously tunable microstrip bandpass filters are developing toward multifunctional integration. For example, researchers prefer to realize filtering and power distribution at the same time, or realize the function of tunable bandpass and stopband in a circuit unit. The tunable microstrip filter design theory can also be verified on-chip, which will provide a new option for full integration of RF front-ends.

REFERENCES

[1] G. Qi, B. van Liempd, P.-I. Mak, R. P. Martins, and J. Craninckx, "A SAW-less tunable RF front end for FDD and IBFD combining an electrical-balance duplexer and a switched-*LC* N-path LNA," *IEEE J. Solid-State Circuits*, vol. 53, no. 5, pp. 1431–1442, May 2018, doi: 10.1109/JSSC.2018.2791477.

[2] A. Nagulu, A. Gaonkar, S. Ahasan, S. Garikapati, T. Chen, G. Zussman, and H. Krishnaswamy, "A full-duplex receiver with true-time-delay cancelers based on switched-capacitor-networks operating beyond the delay-bandwidth limit," *IEEE J. Solid-State Circuits*, vol. 56, no. 5, pp. 1398–1411, May 2021, doi: 10.1109/JSSC.2021.3063658.

[3] D. Psychogiou and K. Sadasivan, "Tunable coaxial cavity resonator-based filters using actuated liquid metal posts," *IEEE Microw. Wireless Compon. Lett.*, vol. 29, no. 12, pp. 763–766, Dec. 2019, doi: 10.1109/LMWC.2019.2950540.

[4] S. Nam, B. Lee, C. Kwak, and J. Lee, "Contactless tuning plunger and its application to K-band frequency-tunable cavity filter," *IEEE Trans. Microw. Theory Techn.*, vol. 67, no. 7, pp. 2713–2719, Jul. 2019, doi: 10.1109/TMTT.2019.2913931.

[5] Z. Yang, R. Zhang, and D. Peroulis, "Design and optimization of bidirectional tunable MEMS all-silicon evanescent-mode cavity filter," *IEEE Trans. Microw. Theory Techn.*, vol. 68, no. 6, pp. 2398–2408, Jun. 2020, doi: 10.1109/TMTT.2020.2976011.

[6] C. M. Thomas and L. E. Larson, "Broadband synthetic transmission-line N-path filter design," *IEEE Trans. Microw. Theory Techn.*, vol. 63, no. 10, pp. 3525–3536, Oct. 2015, doi: 10.1109/TMTT.2015.2473161.

[7] T. B. Herbert, J. S. Hyland, S. Abdullah, J. Wight, and R. E. Amaya, "An active bandpass filter for LTE/WLAN applications using robust active inductors in gallium nitride," *IEEE Trans. Circuits Syst. II, Exp. Briefs*, vol. 68, no. 7, pp. 2252–2256, Jul. 2021, doi: 10.1109/TCSII.2021.3054739.

[8] F. Amin, S. Raman, and K.-J. Koh, "An integrated microwave tunable dual-band Q-enhanced LC band-pass filter in 0.13 μm SiGe BiCMOS," in *Proc. 47th Eur. Microw. Conf. (EuMC)*, Oct. 2017, pp. 33–36, doi: 10.23919/EuMC.2017.8230792.

[9] C.-W. Tang and J.-M. Jiang, "Design of the microstrip bandpass filter with 4 band-switching modes," *IEEE Trans. Circuits Syst. II, Exp. Briefs*, vol. 70, no. 6, pp. 1926–1930, Jun. 2023, doi: 10.1109/TCSII.2022.3229105.

[10] W. S. Tang, S. Y. Zheng, Y. M. Pan, and H. W. Liu, "A frequency independently tunable dual-band bandpass filter with large frequency ratio and ultra-wide stopband," *IEEE Trans. Ind. Electron.*, vol. 70, no. 2, pp. 1894–1904, Feb. 2023, doi: 10.1109/TIE.2022.3161816.

[11] D. Lu, X. Tang, N. S. Barker, and Y. Feng, "Single-band and switchable dual-/single-band tunable BPFs with predefined tuning range, bandwidth, and selectivity," *IEEE Trans. Microw. Theory Techn.*, vol. 66, no. 3, pp. 1215–1227, Mar. 2018, doi: 10.1109/TMTT.2017.2772816.

[12] T. Yang and G. M. Rebeiz, "Bandpass-to-bandstop reconfigurable tunable filters with frequency and bandwidth controls," *IEEE Trans. Microw. Theory Techn.*, vol. 65, no. 7, pp. 2288–2297, Jul. 2017, doi: 10.1109/TMTT.2017.2679182.

[13] S. Arain, P. Vryonides, A. Quddious, and S. Nikolaou, "Reconfigurable BPF with constant center frequency and wide tuning range of bandwidth," *IEEE Trans. Circuits Syst. II, Exp. Briefs*, vol. 67, no. 8, pp. 1374–1378, Aug. 2020, doi: 10.1109/TCSII.2019.2938741.

[14] G. Suo, X. Guo, B. Cao, B. Wei, X. Zhang, T. Zheng, and G. Zhang, "Superconducting varactor tunable filter with constant bandwidth using coupling line," *IEEE Microw. Wireless Compon. Lett.*, vol. 24, no. 9, pp. 628–630, Sep. 2014, doi: 10.1109/LMWC.2014.2330694.

[15] T. Lim, A. Anand, J. Chen, X. Liu, and Y. Lee, "Design method for tunable planar bandpass filters with single-bias control and wide tunable frequency range," *IEEE Trans. Circuits Syst. II, Exp. Briefs*, vol. 68, no. 1, pp. 221–225, Jan. 2021, doi: 10.1109/TCSII.2020.3004614.

[16] A. Zakharov, S. Rozenko, and M. Ilchenko, "Varactor-tuned microstrip bandpass filter with loop hairpin and combline resonators," *IEEE Trans. Circuits Syst. II, Exp. Briefs*, vol. 66, no. 6, pp. 953–957, Jun. 2019, doi: 10.1109/TCSII.2018.2873227.

[17] Z. Zhao, J. Chen, L. Yang, and K. Chen, "Three-pole tunable filters with constant bandwidth using mixed combline and split-ring resonators," *IEEE Microw. Wireless Compon. Lett.*, vol. 24, no. 10, pp. 671–673, Oct. 2014, doi: 10.1109/LMWC.2014.2340996.

[18] C.-F. Chen, G.-Y. Wang, and J.-J. Li, "Microstrip switchable and fully tunable bandpass filter with continuous frequency tuning range," *IEEE Microw. Wireless Compon. Lett.*, vol. 28, no. 6, pp. 500–502, Jun. 2018, doi: 10.1109/LMWC.2018.2831440.

[19] F. Lin and M. Rais-Zadeh, "Continuously tunable 0.55–1.9-GHz bandpass filter with a constant bandwidth using switchable varactor-tuned resonators," *IEEE Trans. Microw. Theory Techn.*, vol. 65, no. 3, pp. 792–803, Mar. 2017, doi: 10.1109/TMTT.2016.2633270.

[20] Y.-H. Cho and G. M. Rebeiz, "Tunable 4-pole noncontiguous 0.7–2.1-GHz bandpass filters based on dual zero-value couplings," *IEEE Trans. Microw. Theory Techn.*, vol. 63, no. 5, pp. 1579–1586, May 2015, doi: 10.1109/TMTT.2015.2409263.

[21] J.-X. Chen, Y. Ma, J. Cai, L.-H. Zhou, Z.-H. Bao, and W. Che, "Novel frequency-agile bandpass filter with wide tuning range and spurious suppression," *IEEE Trans. Ind. Electron.*, vol. 62, no. 10, pp. 6428–6435, Oct. 2015, doi: 10.1109/TIE.2015.2427122.

[22] W. Qin, J. Cai, Y.-L. Li, and J.-X. Chen, "Wideband tunable bandpass filter using optimized varactor-loaded SIRs," *IEEE Microw. Wireless Compon. Lett.*, vol. 27, no. 9, pp. 812–814, Sep. 2017, doi: 10.1109/LMWC.2017.2734848.

[23] L.-H. Zhou, Y.-L. Ma, J. Shi, J.-X. Chen, and W. Che, "Differential dual-band bandpass filter with tunable lower band using embedded DGS unit for common-mode suppression," *IEEE Trans. Microw. Theory Techn.*, vol. 64, no. 12, pp. 4183–4191, Dec. 2016, doi: 10.1109/TMTT.2016.2607176.

[24] X.-K. Bi, T. Cheng, P. Cheong, S.-K. Ho, and K.-W. Tam, "Design of dual-band bandpass filters with fixed and reconfigurable bandwidths based on terminated cross-shaped resonators," *IEEE Trans. Circuits Syst. II, Exp. Briefs*, vol. 66, no. 3, pp. 317–321, Mar. 2019, doi: 10.1109/TCSII.2018.2848667.

[25] W. Feng, Y. Zhang, and W. Che, "Tunable dual-band filter and diplexer based on folded open loop ring resonators," *IEEE Trans. Circuits Syst. II, Exp. Briefs*, vol. 64, no. 9, pp. 1047–1051, Sep. 2017, doi: 10.1109/TCSII.2016.2634555.

[26] J.-X. Chen, M.-Z. Du, Y.-L. Li, Y.-J. Yang, and J. Shi, "Independently tunable/controllable differential dual-band bandpass filters using element-loaded stepped-impedance resonators," *IEEE Trans. Compon., Packag., Manuf. Technol.*, vol. 8, no. 1, pp. 113–120, Jan. 2018, doi: 10.1109/TCPMT.2017.2761789.

[27] Z.-H. Chen and Q.-X. Chu, "Dual-band reconfigurable bandpass filter with independently controlled passbands and constant absolute bandwidths," *IEEE Microw. Wireless Compon. Lett.*, vol. 26, no. 2, pp. 92–94, Feb. 2016, doi: 10.1109/LMWC.2016.2517153.

[28] X. Huang, L. Zhu, Q. Feng, Q. Xiang, and D. Jia, "Tunable bandpass filter with independently controllable dual passbands," *IEEE Trans. Microw. Theory Techn.*, vol. 61, no. 9, pp. 3200–3208, Sep. 2013, doi: 10.1109/TMTT.2013.2273894.

[29] M. Ohira, S. Hashimoto, Z. Ma, and X. Wang, "Coupling-matrix-based systematic design of single-DC-bias-controlled microstrip higher order tunable bandpass filters with constant absolute bandwidth and transmission zeros," *IEEE Trans. Microw. Theory Techn.*, vol. 67, no. 1, pp. 118–128, Jan. 2019, doi: 10.1109/TMTT.2018.2873366.

[30] W.-J. Zhou and J.-X. Chen, "High-selectivity tunable balanced bandpass filter with constant absolute bandwidth," *IEEE Trans. Circuits Syst. II, Exp. Briefs*, vol. 64, no. 8, pp. 917–921, Aug. 2017, doi: 10.1109/TCSII.2016.2621120.

[31] C. Ge and X.-W. Zhu, "Highly-selective tunable bandpass filter with two-path mixed coupling," *IEEE Microw. Wireless Compon. Lett.*, vol. 24, no. 7, pp. 451–453, Jul. 2014, doi: 10.1109/LMWC.2014.2316218.

[32] B. You, L. Chen, Y. Liang, and X. Wen, "A high-selectivity tunable dual-band bandpass filter using stub-loaded stepped-impedance resonators," *IEEE Microw. Wireless Compon. Lett.*, vol. 24, no. 11, pp. 736–738, Nov. 2014, doi: 10.1109/LMWC.2014.2348322.

[33] H. Zhu and A. M. Abbosh, "Tunable balanced bandpass filter with wide tuning range of center frequency and bandwidth using compact coupled-line resonator," *IEEE Microw. Wireless Compon. Lett.*, vol. 26, no. 1, pp. 7–9, Jan. 2016, doi: 10.1109/LMWC.2015.2505647.

[34] X. Luo, S. Sun, and R. B. Staszewski, "Tunable bandpass filter with two adjustable transmission poles and compensable coupling," *IEEE Trans. Microw. Theory Techn.*, vol. 62, no. 9, pp. 2003–2013, Sep. 2014, doi: 10.1109/TMTT.2014.2337287.

[35] J.-R. Mao, W.-W. Choi, K.-W. Tam, W. Q. Che, and Q. Xue, "Tunable bandpass filter design based on external quality factor tuning and multiple mode resonators for wideband applications," *IEEE Trans. Microw. Theory Techn.*, vol. 61, no. 7, pp. 2574–2584, Jul. 2013, doi: 10.1109/TMTT.2013.2264684.

[36] D. Lu, X. Tang, N. S. Barker, M. Li, and T. Yan, "Synthesis-applied highly selective tunable dual-mode BPF with element-variable coupling matrix," *IEEE Trans. Microw. Theory Techn.*, vol. 66, no. 4, pp. 1804–1816, Apr. 2018, doi: 10.1109/TMTT.2017.2783376.

[37] S.-X. Zhang, Z.-H. Chen, and Q.-X. Chu, "Compact tunable balanced bandpass filter with novel multi-mode resonator," *IEEE Microw. Wireless Compon. Lett.*, vol. 27, no. 1, pp. 43–45, Jan. 2017, doi: 10.1109/LMWC.2016.2629965.

[38] M. Fan, K. Song, and Y. Fan, "Reconfigurable bandpass filter with wide-range bandwidth and frequency control," *IEEE Trans. Circuits Syst. II, Exp. Briefs*, vol. 68, no. 6, pp. 1758–1762, Jun. 2021, doi: 10.1109/TCSII.2020.3040190.

[39] B.-F. Zong, G.-M. Wang, J.-G. Liang, and C. Zhou, "Compact bandpass filter with two tunable transmission zeros using hybrid resonators," *IEEE Microw. Wireless Compon. Lett.*, vol. 25, no. 2, pp. 88–90, Feb. 2015, doi: 10.1109/LMWC.2014.2382673.

[40] C.-W. Tang, C.-T. Tseng, and S.-C. Chang, "A tunable bandpass filter with modified parallel-coupled line," *IEEE Microw. Wireless Compon. Lett.*, vol. 23, no. 4, pp. 190–192, Apr. 2013, doi: 10.1109/LMWC.2013.2247585.

[41] H.-J. Tsai, B.-C. Huang, N.-W. Chen, and S.-K. Jeng, "A reconfigurable bandpass filter based on a varactor-perturbed, T-shaped dual-mode resonator," *IEEE Microw. Wireless Compon. Lett.*, vol. 24, no. 5, pp. 297–299, May 2014, doi: 10.1109/LMWC.2014.2306893.

[42] T.-C. Lee, J. Lee, and D. Peroulis, "Dynamic bandpass filter shape and interference cancellation control utilizing bandpass–bandstop filter cascade," *IEEE Trans. Microw. Theory Techn.*, vol. 63, no. 8, pp. 2526–2539, Aug. 2015, doi: 10.1109/TMTT.2015.2447511.

[43] P.-L. Chi, T. Yang, and T.-Y. Tsai, "A fully tunable two-pole bandpass filter," *IEEE Microw. Wireless Compon. Lett.*, vol. 25, no. 5, pp. 292–294, May 2015, doi: 10.1109/LMWC.2015.2409794.

[44] N. Kumar, S. Narayana, and Y. K. Singh, "Constant absolute bandwidth tunable symmetric and asymmetric bandpass responses based on reconfigurable transmission zeros and bandwidth," *IEEE Trans. Circuits Syst. II, Exp. Briefs*, vol. 69, no. 3, pp. 1014–1018, Mar. 2022, doi: 10.1109/TCSII.2021.3125575.

[45] Y. Song, G.-M. Yang, and W. Geyi, "Compact UWB bandpass filter with dual notched bands using defected ground structures," *IEEE Microw. Wireless Compon. Lett.*, vol. 24, no. 4, pp. 230–232, Apr. 2014, doi: 10.1109/LMWC.2013.2296291.

[46] H. Shaman and J.-S. Hong, "A novel ultra-wideband (UWB) bandpass filter (BPF) with pairs of transmission zeroes," *IEEE Microw. Wireless Compon. Lett.*, vol. 17, no. 2, pp. 121–123, Feb. 2007, doi: 10.1109/LMWC.2006.890335.

[47] K. Song and Q. Xue, "Compact ultra-wideband (UWB) bandpass filters with multiple notched bands," *IEEE Microw. Wireless Compon. Lett.*, vol. 20, no. 8, pp. 447–449, Aug. 2010, doi: 10.1109/LMWC.2010.2050303.

[48] L. Kurra, M. P. Abegaonkar, A. Basu, and S. K. Koul, "Switchable and tunable notch in ultra-wideband filter using electromagnetic bandgap structure," *IEEE Microw. Wireless Compon. Lett.*, vol. 24, no. 12, pp. 839–841, Dec. 2014, doi: 10.1109/LMWC.2014.2363020.

[49] H. Wang, K.-W. Tam, S.-K. Ho, W. Kang, and W. Wu, "Design of ultra-wideband bandpass filters with fixed and reconfigurable notch bands using terminated cross-shaped resonators," *IEEE Trans. Microw. Theory Techn.*, vol. 62, no. 2, pp. 252–265, Feb. 2014, doi: 10.1109/TMTT.2013.2296530.

[50] Z. Wu, Y. Shim, and M. Rais-Zadeh, "Miniaturized UWB filters integrated with tunable notch filters using a silicon-based integrated passive device technology," *IEEE Trans. Microw. Theory Techn.*, vol. 60, no. 3, pp. 518–527, Mar. 2012, doi: 10.1109/TMTT.2011.2178428.

[51] C. Teng, P. Cheong, and K.-W. Tam, "Reconfigurable wideband bandpass filters based on dual cross-shaped resonator," in *IEEE MTT-S Int. Microw. Symp. Dig.*, May 2019, pp. 1–3, doi: 10.1109/IEEE-IWS.2019.8804159.

[52] D. Psychogiou, R. Gómez-García, and D. Peroulis, "RF wide-band bandpass filter with dynamic in-band multi-interference suppression capability," *IEEE Trans. Circuits Syst. II, Exp. Briefs*, vol. 65, no. 7, pp. 898–902, Jul. 2018, doi: 10.1109/TCSII.2017.2726145.

[53] D. Psychogiou, R. Gómez-García, and D. Peroulis, "Wide-passband filters with in-band tunable notches for agile multi-interference suppression in broad-band antenna systems," in *Proc. IEEE Radio Wireless Symp. (RWS)*, Jan. 2018, pp. 213–216, doi: 10.1109/RWS.2018.8304990.

[54] X. Zhu, T. Yang, P.-L. Chi, and R. Xu, "Novel tunable isolation network used in ring-type single-to-balanced, power-dividing, and single-ended filter with arbitrary power-division ratios," *IEEE Trans. Microw. Theory Techn.*, vol. 68, no. 2, pp. 666–680, Feb. 2020, doi: 10.1109/TMTT.2019.2949787.

[55] D. Psychogiou and R. Gómez-García, "Reflectionless adaptive RF filters: Bandpass, bandstop, and cascade designs," *IEEE Trans. Microw. Theory Techn.*, vol. 65, no. 11, pp. 4593–4605, Nov. 2017, doi: 10.1109/TMTT.2017.2734086.

[56] S.-W. Jeong, T.-H. Lee, and J. Lee, "Frequency- and bandwidth-tunable absorptive bandpass filter," *IEEE Trans. Microw. Theory Techn.*, vol. 67, no. 6, pp. 2172–2180, Jun. 2019, doi: 10.1109/TMTT.2019.2914111.

[57] M. Fan, K. Song, L. Yang, and R. Gómez-Garcia, "Frequency-reconfigurable input-reflectionless bandpass filter and filtering power divider with constant absolute bandwidth," *IEEE Trans. Circuits Syst. II, Exp. Briefs*, vol. 68, no. 7, pp. 2424–2428, Jul. 2021, doi: 10.1109/TCSII.2021.3049417.

[58] M. Fan, K. Song, L. Yang, and R. Gómez-García, "Frequency-tunable constant-absolute-bandwidth single-/dual-passband filters and diplexers with all-port-reflectionless behavior," *IEEE Trans. Microw. Theory Techn.*, vol. 69, no. 2, pp. 1365–1377, Feb. 2021, doi: 10.1109/TMTT.2020.3040481.

[59] Z. Cao, X. Bi, and Q. Xu, "Tunable reflectionless filter with independently controllable dual passbands and absorbed harmonic signals," *IEEE Trans. Circuits Syst. II, Exp. Briefs*, vol. 68, no. 11, pp. 3416–3420, Nov. 2021, doi: 10.1109/TCSII.2021.3076499.

[60] N. Kumar and Y. K. Singh, "Compact constant bandwidth tunable wideband BPF with second harmonic suppression," *IEEE Microw. Wireless Compon. Lett.*, vol. 26, no. 11, pp. 870–872, Nov. 2016, doi: 10.1109/LMWC.2016.2615001.

[61] D. Tang, H. J. Qian, Y. Dong, and X. Luo, "Compact 1.75–2.7 GHz tunable BPF with wide stopband up to 9.5 GHz using harmonic-controlled SIDGS resonators," *IEEE Trans. Circuits Syst. II, Exp. Briefs*, vol. 69, no. 11, pp. 4228–4232, Nov. 2022, doi: 10.1109/TCSII.2022.3185805.
[62] G. Chaudhary, Y. Jeong, and J. Lim, "Harmonic suppressed dual-band bandpass filters with tunable passbands," *IEEE Trans. Microw. Theory Techn.*, vol. 60, no. 7, pp. 2115–2123, Jul. 2012, doi: 10.1109/TMTT.2012.2197020.
[63] G. Chaudhary, Y. Jeong, and J. Lim, "Dual-band bandpass filter with independently tunable center frequencies and bandwidths," *IEEE Trans. Microw. Theory Techn.*, vol. 61, no. 1, pp. 107–116, Jan. 2013, doi: 10.1109/TMTT.2012.2222910.

MENGJIE QIN received the B.S. degree in communication engineering from Henan University, Henan, China, in 2020. She is currently pursuing the Ph.D. degree in microelectronics and solid-state electronics with the University of Chinese Academy of Sciences, Beijing, China. Her current research interests include the tunable passive circuits, RF/microwave integrated circuits, and analog integrated circuits.

ZHONGMAO LI (Member, IEEE) received the M.S. degree from Yunnan University, Kunming, Yunnan, China, in 2014, and the Ph.D. degree in microelectronics from the University of Chinese Academy of Sciences, Beijing, China, in 2022. Since 2014, he has been with the Institute of Microelectronics, Chinese Academy of Sciences. His research interests include the areas of microwave integrated circuits, active and passive microwave devices, receiver systems, and computational electromagnetics.

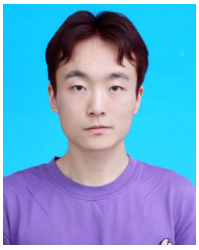

ZHIPENG REN received the B.S. degree in electronic science and technology from Xi'an Jiaotong University (XJTU), Xi'an, Shanxi, in 2023. He is currently pursuing the M.S. degree in microelectronics and solid-state electronics with the University of Chinese Academy of Sciences (UCAS), Beijing, China. His research interests include analog integrated circuit design technology and RF integrated circuit design technology.

PENGZHAN LIU (Student Member, IEEE) was born in Henan, China. He received the B.S. degree in communication engineering from Shandong University of Technology, Shandong, in 2019. He is currently pursuing the Ph.D. degree in microelectronics and solid-state electronics with the University of Chinese Academy of Sciences, Beijing, China. His current research interests include RF/microwave integrated circuits and miniaturized passive circuits.

LANLAN LIAO received the B.S. degree in energy and power engineering from Guangxi University, Nanning, China, in 2021. She is currently pursuing the M.S. degree in communication engineering with Zhengzhou University, Zhengzhou, China. She is also a joint training student with the Institute of Microelectronics, Chinese Academy of Sciences. Her primary research interests include the design of substrate integrated waveguide (SIW) filtering crossovers and its application in the microwave field.

XIN QIU received the M.Eng. degree from Guilin University of Electronic Technology, Guilin, China, in 2003, and the Ph.D. degree from the Chinese Academy of Sciences, Beijing, China, in 2008. He is currently a Research Fellow with the Institute of Microelectronics, Chinese Academy of Sciences, Beijing, where he leads the Research Center of Communications and Information Engineering. His research interests include wireless communications, 5G/6G, and digital signal processing in communication.

ZHIQIANG LI (Member, IEEE) received the B.S. degree in microelectronics from Jilin University, Changchun, China, in 2004, and the Ph.D. degree in microelectronics from the University of Chinese Academy of Sciences, Beijing, China, in 2009. From 2015 to 2016, he was a Visiting Professor in electrical and computer engineering with the University of California at Santa Barbara, Santa Barbara, CA, USA. He is currently a Professor with the Institute of Microelectronics, Chinese Academy of Sciences, Beijing. His current research interests include semiconductor device and process simulation electronic design automation (EDA) tools, and radio frequency integrated circuits design.